Journal of Catalysis 262 (2009) 35–43

Contents lists available at ScienceDirect

Journal of Catalysis

www.elsevier.com/locate/jcat

Selective propane oxidation over MoVSbO catalysts. On the preparation, characterization and catalytic behavior of M1 phase

Francisco Ivars [a], Benjamín Solsona [b], Enrique Rodríguez-Castellón [c], José M. López Nieto [a,*]

[a] Instituto Universitario Mixto de Tecnología Química (UPV-CSIC), Avda. Los Naranjos s/n, 46022 Valencia, Spain
[b] Departamento de Ingeniería Química, Universidad de Valencia, Dr. Moliner 50, 46100 Burjassot, Spain
[c] Departmento Química Inorgánica, Facultad de Ciencias, Universidad de Málaga, 29071 Málaga, Spain

ARTICLE INFO

Article history:
Received 1 August 2008
Revised 21 November 2008
Accepted 21 November 2008
Available online 24 December 2008

Keywords:
Hydrothermal synthesis
Post-synthesis treatment
Mo–V–Sb mixed oxides
M1 phase
Propane oxidation

ABSTRACT

Nb-free $(SbO)_2M_{20}O_{56}$ catalysts (M = Mo, V) presenting pure M1 phase have been prepared by a post-synthesis treatment with hydrogen peroxide of a heat-treated MoVSbO mixed metal oxide catalyst previously prepared by hydrothermal method. The characterization of catalysts and their results for propane oxidation suggest that the optimization in the preparation of the M1 phase depends strongly on the washing procedure. The optimal removing of Sb species formed during post-synthesis treatment can explain the improvement in the catalytic activity; while the better selectivity to acrylic acid of the catalysts obtained by post-synthesis treatment can be explained by the elimination of M2 phase and the modification of the M1 phase crystals surface. The importance of M1 phase in the catalytic performance during the selective propane oxidation over Nb-free Mo–V–Sb based catalysts is also discussed.

© 2008 Elsevier Inc. All rights reserved.

1. Introduction

The functionalization of light alkanes is a challenging matter since they present a comparatively low price and the exploration of new catalytic systems for the oxidation of short chain alkanes in gas phase has special interest from both fundamental and industrial point of view [1–5]. However, only since mid 90's promising catalytic results began to emerge. This is the case of Mo–V–Te(Sb)–Nb–O mixed oxides, initially reported by Mitsubishi [6], which are the most effective catalysts in the (amm)oxidation of propane [6–8] and in the oxidative dehydrogenation (ODH) of ethane to ethylene [9–11], presenting, moreover, an interesting selectivity to partial oxidation products during the oxidation of *n*-butane [12].

Typically, MoVTeNb-based catalysts present as main crystalline phases [8,13–25]: (i) orthorhombic $(TeO)_2M_{20}O_{56}$ (M = Mo, V, Nb), also called M1; and (ii) orthorhombically distorted HTB-type phase $Te_{0.33}MO_{3.33}$ (M = Mo, V, Nb), also called M2. In addition, other phases as $TeMo_5O_{16}$ or (V, Nb)-containing Mo_5O_{14}, or TTB-bronzes can also be observed depending on the catalyst preparation procedure [16].

Mo–V–Sb-based catalysts have also been reported as efficient catalysts in the oxidation of propane to acrylic acid [18,23,25–32] and in the ODH of ethane [33] most of them presenting crystalline phases similar to those observed in Te-containing catalysts: (i) $(SbO)_2M_{20}O_{56}$ (with M = Mo, V, Nb) as the M1-like phase [26], and (ii) $(Sb_2O)M_6O_{19}$ (with M = Mo, V, Nb) as the M2-like phase [26].

The presence of Nb ions in both Te- and Sb-containing catalysts [6–34] favors an improvement in the selective oxidation reactions. This effect has been clearly explained by a better stability of acrylic acid on Nb-containing catalysts [15], as a consequence of the low number/strength of acid sites in these catalysts [34].

On the other hand, a synergetic effect for propane oxidation between M1 and M2 phases has been proposed for MoVTeNbO catalysts [24,25], which is not clear for the corresponding Sb-containing catalysts [25]. This different behavior between Te- and Sb-containing catalysts could be due to the different performance of their corresponding M2 phases [25,30,35]. Moreover, and although it has been demonstrated that the incorporation of potassium with the elimination of acid sites improves the formation of acrylic acid [30,31], the role of the M1 and M2 phases in Nb-free MoVSbO catalysts is still under discussion.

Pure M1 phase can be obtained directly by hydrothermal synthesis [19,21–23] or by a post-synthesis treatment of the corresponding mixed metal oxides [25,36,37], although in most of these cases, the preparation of the M1 phase takes place when Nb is present in the catalysts.

In this paper we present a comparative study on the selective oxidation of propane to acylic acid over Nb-free MoVSbO catalysts presenting pure and mixed M1 and M2 phases. The mixed phases of MoVSbO were prepared hydrothermally, while the pure M1 phase was obtained by a post-synthesis treatment with an

* Corresponding author. Fax: +34 963877809.
E-mail address: jmlopez@itq.upv.es (J.M. López Nieto).

0021-9517/$ – see front matter © 2008 Elsevier Inc. All rights reserved.
doi:10.1016/j.jcat.2008.11.021

Table 1
Physico-chemical characteristics of MoVSb mixed metal oxide catalysts.

Catalyst	EDX composition Mo/V/Sb	S_{BET} (m^2/g)	NH_3-TPD			Phases detected by XRD[c]
			Acid sites[a]		T_{max}[b] (°C)	
			(μmol/g)	(μmol/m^2)		
A-1	1/0.27/0.28	20.6	154	8	212	M1, Sb-rich mixed oxide
A-2	1/0.26/0.17	18.2	156	8	190	M1, Sb-rich mixed oxide
A-3	1/0.24/0.16	15.8	129	8	182	M1
HT-1	1/0.27/0.15	13.2	320	24	212	M1, M2
HT-2	1/0.35/0.50	3.4	3.7	1	165	M2
A-3W	0.02–0.01/0/1	–	–	–	–	Sb-rich mixed oxide

[a] Amount of ammonia chemisorbed at 100 °C during the NH_3-TPD experiment, per gram or per surface area of catalyst (measured in standard temperature and pressure).
[b] T_{max}, temperature of maximum desorption observed in the NH_3-TPD experiments.
[c] M1 phase = $(SbO)_2M_{20}O_{56}$; M2 phase = $(Sb_2O)M_6O_{19}$ (M = Mo, V); Sb-rich mixed oxide = $Mo_{0.01-0.02}SbO_{1.9-3.3}\cdot xH_2O$ (determined by EDS) which presents XRD pattern very similar to that of a phase previously reported, $Mo_{0.32}SbO_{3.3}\cdot xH_2O$ (JCPDS: 44-0054).

aqueous solution of hydrogen peroxide [25]. Finally, the role of M1 and M2 phases in MoVSbO mixed oxide catalysts during the selective oxidation of propane to acrylic acid as well as the importance of the procedure used in the preparation of M1 phase are discussed.

2. Experimental

2.1. Catalysts preparation

A MoVSbO mixed metal oxide, containing both M1 and M2 phases, has been prepared hydrothermally from a gel with vanadyl sulfate, antimony sulfate, ammonium heptamolybdate and water with a Mo/V/Sb atomic ratio of 1/0.18/0.15 according to the procedure previously reported [30]. The gel obtained was introduced in Teflon-line stainless steel autoclave at 175 °C for 48 h. The resulting solid was filtered, washed and dried at 100 °C for 12 h. Finally, the solid was heat-treated at 600 °C for 2 h in flowing N_2. This sample will be named as **HT-1**.

Pure M1-like catalysts were prepared by washing the **HT-1** sample according to the following procedure: the solid was treated at room temperature with an aqueous solution of 15 wt% hydrogen peroxide for 5 h under vigorous stirring, filtered and washed with distilled water. Three different samples were achieved by washing treated sample **HT-1** with 1, 2 or 3 cycles (100 $ml_{H_2O}\,g^{-1}_{cat.}$ each cycle), and the resulting solids were heated at 500 °C for 2 h in N_2 stream. These catalysts have been named as **A-1**, **A-2** and **A-3**, respectively. In addition, the turbid mother liquids obtained in each case after filtering and washing, were separately centrifuged in order to recover the solid in suspension. These solids were dried at 100 °C and named as **A-1W**, **A-2W** and **A-3W**, respectively.

For comparison, pure M2-like catalysts were also prepared hydrothermally by using a gel with a Mo/V/Sb atomic ratio of 1/0.5/0.5. The sample heat-treated at 600 °C in N_2 will be named as **HT-2**. The characteristics of catalysts are presented in Table 1.

2.2. Catalysts characterization

BET specific surface areas were measured on a Micromeritics TriStar 3000 instrument, with adsorption of N_2 at 77.300 K.

X-ray diffraction patterns (XRD) were collected using a Philips X'Pert diffractometer equipped with a graphite monochromator, operating at 40 kV and 45 mA and employing nickel-filtered CuK_α radiation ($\lambda = 0.1542$ nm).

Scanning electron microscopy (SEM) and energy dispersive X-ray spectrometry microanalysis (EDX) were performed on a JEOL JSM 6300 LINK ISIS instrument. The quantitative EDX analyses were performed using an Oxford LINK ISIS System with the SEMQUANT program, which introduces the ZAF correction.

Transmission electron microscopy images were obtained on a Philips CM10 electron microscope operating at 100 kV. The samples were prepared by dispersing the powder products in pure ethanol and transferred to carbon-coated copper grids.

Infrared spectra were recorded at room temperature in the 300–3900 cm^{-1} region with a Nicolet 205xB spectrophotometer, equipped with a Data Station, at a spectral resolution of 1 cm^{-1} and accumulations of 128 scans. The pellets were prepared with 20 mg of sample mixed with 100 mg of dry KBr and pressed into a disk.

Temperature programmed desorption of ammonia (NH_3-TPD) experiments were carried out on a TPD/2900 apparatus from Micromeritics. 300 mg of sample was pre-treated in an Ar stream at 450 °C for 1 h. Ammonia was chemisorbed by pulses at 100 °C until equilibrium was reached. Then, the sample was fluxed with He stream for 15 min, prior to increase the temperature up to 500 °C in a helium stream of 100 $ml\,min^{-1}$ and using a heating rate of $10\,°C\,min^{-1}$. The NH_3 desorption was monitored with a thermal conductivity detector (TCD) and a mass-spectrometer. The measures were at standard pressure and temperature.

X-ray photoelectron spectra were collected using a Physical Electronics PHI 5700 spectrometer with non-monochromatic MgK_α radiation (300 W, 15 kV, 1253.6 eV) for the analysis of photoelectronic signals of C 1*s*, O 1*s*, V 2*p*, Mo 3*d*, and Sb 3*d* and with a multi-channel detector. Spectra of powdered samples were recorded with the constant pass energy values at 29.35 eV, using a 720 μm diameter analysis area. Under these conditions, the Au $4f_{7/2}$ line was recorded with 1.16 eV FWHM at a binding energy of 84.0 eV. The spectrometer energy scale was calibrated by using the Cu $2p_{3/2}$, Ag $3d_{5/2}$ and Au $4f_{7/2}$ photoelectron lines at 932.7, 368.3 and 84.0 eV, respectively. During data processing of the XPS spectra, binding energy values were referenced to the C 1*s* peak (284.8 eV) from the adventitious contamination layer. The PHI ACCESS ESCA-V6.0 F software package was used for acquisition and data analysis. A Shirley-type background was subtracted from the signals. Recorded spectra were always fitted using Gauss–Lorentz curves, in order to determine the binding energy of the different element core levels more accurately. The error in BE was estimated to be *ca.* 0.1 eV. Short acquisition time of 10 min was used to examine C 1*s*, V 2*p* regions in order to avoid, as much as possible, photo-reduction of V^{5+} species. Satellite subtraction was always performed to study the V 2*p* region.

2.3. Catalytic tests

The catalytic experiments were carried out at atmospheric pressure, in the 340–400 °C temperature range, using a fixed bed quartz tubular reactor (i.d. 20 mm; length 400 mm). Catalyst samples were introduced in the reactor diluted with silicon carbide in

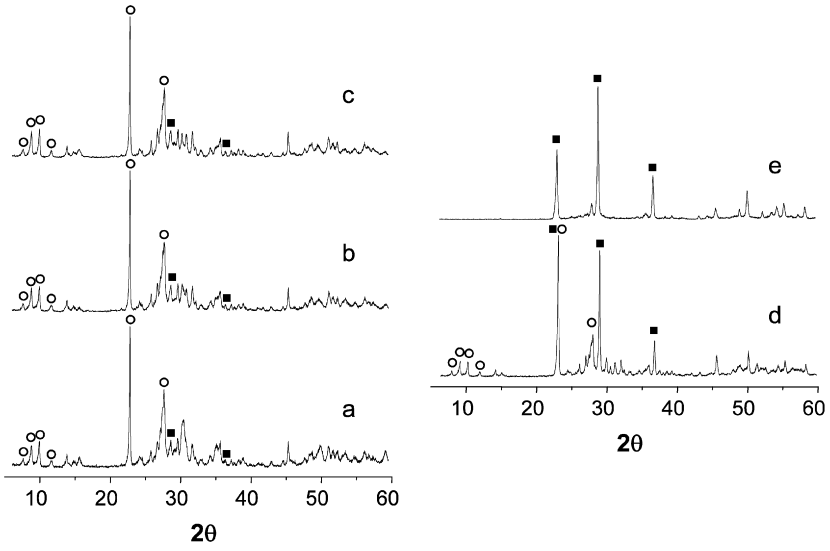

Fig. 1. XRD patterns of MoVSbO based catalysts: (a) **A-1**; (b) **A-2**; (c) **A-3**; (d) **HT-1**; (e) **HT-2**. Symbols: (○) $(SbO)_2M_{20}O_{56}$; (■) $(Sb_2O)M_6O_{19}$.

order to keep a constant volume in the catalytic bed. The feed consisted in a mixture of $C_3H_8/O_2/He/H_2O$ or $C_3H_6/O_2/He/H_2O$ with molar ratios of 4/8/58/30 or 1.7/6.8/76.5/15, respectively. Reactants and products were analyzed by online gas chromatography using two packed columns: (i) Molecular sieve 5 Å (3 m); and (ii) Porapak Q (3 m). Blank runs showed no conversion in the temperature range studied [19,30].

3. Results and discussion

3.1. Characterization results

Table 1 shows the physico-chemical characteristics of catalysts. M1-like catalysts, i.e. **A**-series, present surface areas from 15 to 21 $m^2\,g^{-1}$, with the less washed sample (**A-1** catalyst) showing the highest surface area. We must indicate that sample **HT-1** (mixed M1 and M2 phases) presents a BET surface area of 13.2 $m^2\,g^{-1}$, whereas sample **HT-2** (M2-like phase) presents the lowest surface area (below 4 $m^2\,g^{-1}$).

The Mo/V/Sb atomic ratios of catalysts determined by SEM-EDX microanalyses are also presented in Table 1. The EDX results for **HT-1** and **HT-2** catalysts were very close to those previously reported for similar catalysts [30]. Moreover, the composition of catalysts of the **A**-series strongly depends on the washing conditions. Thus, the samples washed during three cycles (**A-3** catalyst) presented the lowest Sb/Mo ratio, while the sample washed during one cycle (**A-1** catalyst) presented the highest Sb/Mo ratio. Thus, the Sb-enrichment observed for sample **A-1** decreases in the sample washed during three cycles (sample **A-3**).

XRD patterns of **A**-series catalysts are presented in Fig. 1. For comparison, the XRD pattern of sample **HT-1** (showing the characteristic peaks of both $(SbO)_2M_{20}O_{56}$ and $(Sb_2O)M_6O_{19}$ crystalline phases [26,30]), and sample **HT-2** (presenting only the characteristic peaks of $(Sb_2O)M_6O_{19}$ crystallites [26,30]) have been also included.

In the case of **A**-series catalysts, $(SbO)_2M_{20}O_{56}$ was the crystalline phase mainly observed (Fig. 1, patterns a, b and c). Thus, we can conclude that the post-synthesis treatment with an aqueous solution of hydrogen peroxide leads to the selective removal of the M2 phase from MoVSbO catalysts containing M1 and M2 phase mixtures. However, additional diffraction peaks have been observed in XRD patterns of these catalysts and especially in the less washed sample, i.e. **A-1** catalyst (Fig. 1, pattern a).

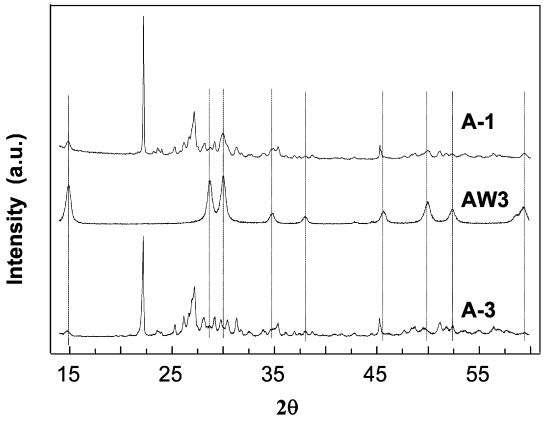

Fig. 2. XRD patterns of **A-1** and **A-3** catalysts, and **AW3** (solid obtained from mother liquids of washing **A-3** catalyst). Dashed lines are the characteristic diffraction peaks of $Mo_{0.32}SbO_{3.3}\cdot xH_2O$ (JCPDS: 44-0054).

In order to determine the nature of these new peaks, the solids recovered from the washing mother liquids obtained after washing the **A**-series solids have been also studied by XRD. It must be indicated that these solids (**A-1W**, **A-2W** and **A-3W**) presented a similar XRD pattern, although the amount of solid recovered increased with the number of washing cycles.

Fig. 2 compares the XRD pattern of the solid **A-3W**, with that of **A-3** and **A-1** catalysts. Accordingly, it can be concluded that the appearance of small reflections at $2\theta = 14.9$, 28.6, 29.9, 34.7, 37.9, 45.9, 49.9, 52.4, 59.3° in catalyst **A-1** corresponds to the presence of a Sb-rich mixed oxide phase with a structure similar to $Mo_{0.32}SbO_{3.3}\cdot xH_2O$ (JCPDS: 44-0054) but with a Sb loading higher, as it has been observed by SEM/EDX analysis: $Mo_{0.01-0.02}SbO_{1.9-3.3}\cdot xH_2O$. This Sb-rich phase is mainly observed in the solid recovered (**A-3W**) from mother liquids of washing **A-3** (Fig. 2). Thus, the amount of $Mo_{0.01-0.02}SbO_{1.9-3.3}\cdot xH_2O$ on the surface of M1 phase crystals of **A**-series catalysts, is in good agreement with the Sb/Mo ratio observed by EDX in **A-1** to **A-3** samples. The lower the number of washing cycles the higher is the Sb/Mo ratio, being the catalyst **A-1** the one with the highest Sb/Mo molar ratio.

On the other hand, we must indicate that the unit cell parameters of phase M1, i.e. **a** (nm) = 21.022; **b** (nm) = 26.666; **c** (nm) = 4.012, in the **A-3** catalyst are in good agreement to those previously reported for Te- or Sb-samples presenting M1 phase

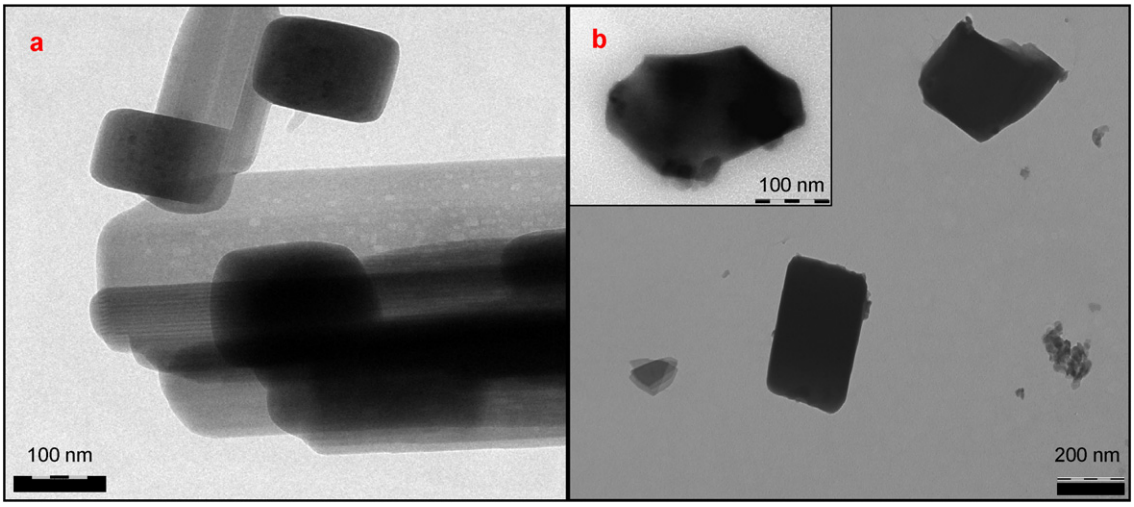

Fig. 3. TEM micrographs of MoVSbO catalysts: (a) **HT-1**; (b) **HT-2**.

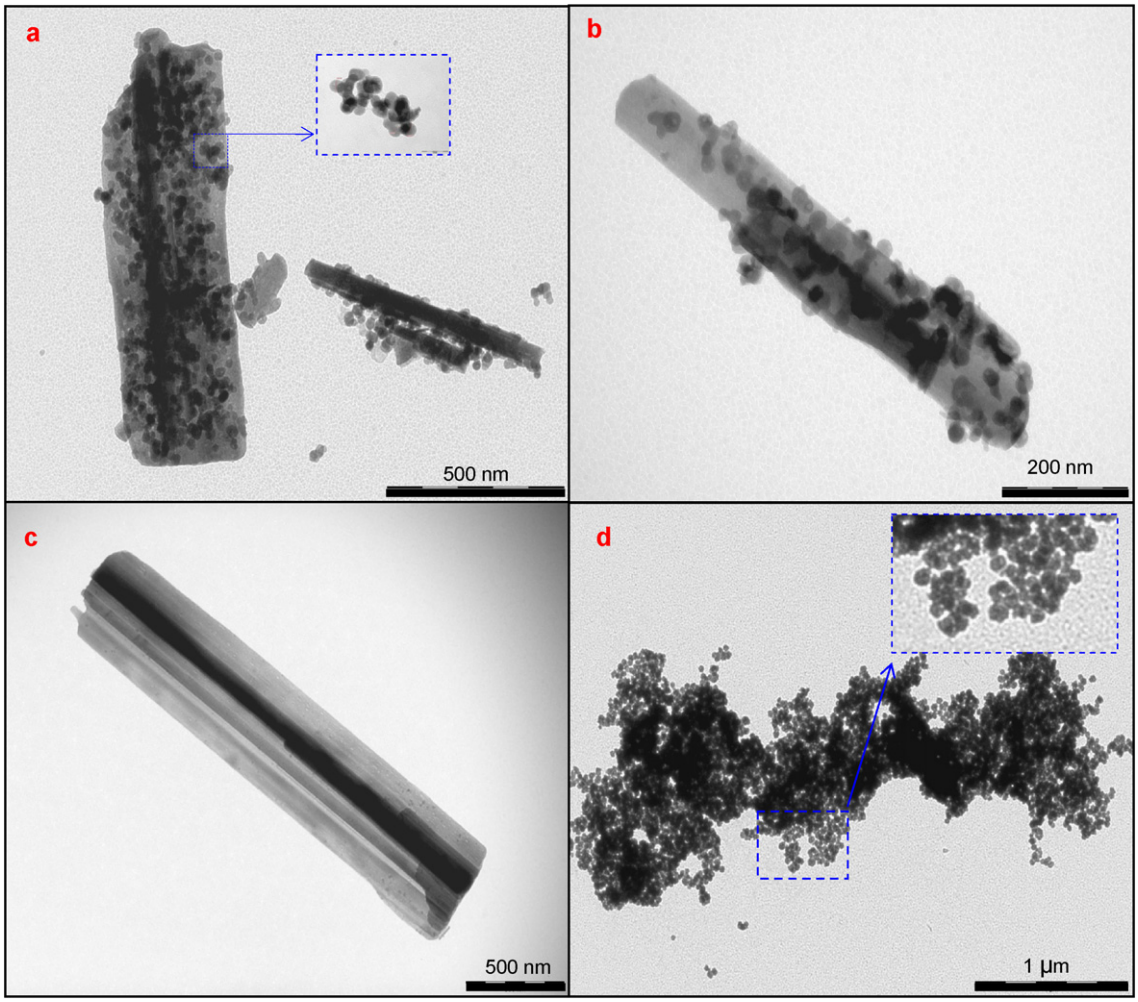

Fig. 4. TEM micrographs of MoVSbO catalysts: (a) **A-1**; (b) **A-2**; and (c) **A-3**. For comparison, TEM micrography of **A-3W** (centrifuged solid obtained from the mother liquids of washing sample **A-3**) is also included (d).

[13,14,26,38]. The unit cell parameters for M1 phase of **A-1** and **A-2** catalysts resulted to be almost identical to those of **A-3** catalyst.

The TEM micrographs of catalysts are presented in Figs. 3 and 4. The TEM image of sample **HT-1** (Fig. 3a) is characterized by the presence of both needle-like crystals (with length between 500 nm and 2 µm) and compact crystals (with length between 100 nm and 200 nm). The sample **HT-2** (Fig. 3b) only presents very compact crystals (with length between 300 nm and 1500 nm) corresponding to M2 phase crystals, as observed by XRD.

Fig. 4 shows some TEM pictures of catalysts **A-1**, **A-2** and **A-3**. For comparison, TEM micrography of **A-3W** (centrifuged solid ob-

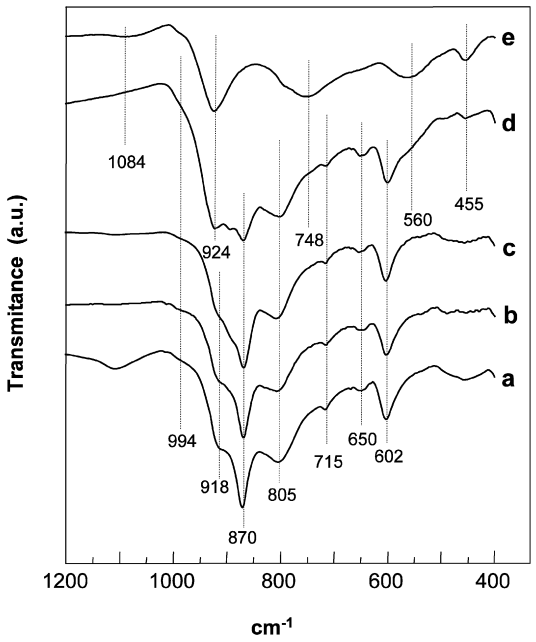

Fig. 5. FT-IR spectra of MoVSbO based catalysts: (a) **A-1**; (b) **A-2**; (c) **A-3**; (d) **HT-1**; (e) **HT-2**.

tained from the mother liquids of washing sample **A-3**) is also included (Fig. 4d).

Samples **A-1** to **A-3** present needle-like shape crystals (with length between 500 nm and 2 μm), corresponding to the orthorhombic $(SbO)_2M_{20}O_{56}$ phase (observed by XRD), which suggest that this phase shows a preferential growth in the *c* axis direction [0, 0, 1]. However, we must inform the presence of nanoparticles (diameter of particle within range 20–30 nm, with a spherical morphology) surrounding the former structure, whose amount decreases when increasing the number of washing cycles. Accordingly, **A-1** catalyst shows the highest amount of these nanospheres over M1-like crystals surface (Fig. 4a), while these ones are almost absent in **A-3** catalyst (Fig. 4c).

TEM micrographs of the solid **A-3W** (Fig. 4d), recovered from washing mother liquids of sample **A-3**, show the same morphology that those nanoparticles surrounding the M1 crystals in samples with a lower number of washing cycles, i.e. **A-1** and **A-2.** According to the XRD and SEM/EDX results (Fig. 1 and Table 1), it can be concluded that $Mo_{0.01-0.02}SbO_{1.9-3.3}{\cdot}xH_2O$ nanospheres are deposited on the surface of M1 phase crystals during the post-synthesis treatment when the catalyst is not washed enough. This fact can explain the results shown in Table 1, in which the BET surface area of washed samples decreases when increasing the number of washing cycles, probably as a consequence of the elimination of Sb-rich nanospheres supported over M1 phase crystals. In addition, these results can also explain the higher Sb/Mo ratio of **A-1** catalyst compared to **HT-1**, since the stoichiometries of the nanoparticles ($Mo_{0.01-0.02}SbO_{1.9-3.3}{\cdot}xH_2O$) present a Sb-loading around 150–300 and 500–1000 times higher than M2 and M1 phases, respectively. As can be seen in Fig. 4a, the nanospheres recovering the M1 crystallite have a relative important contribution respect to the size of the M1 crystallite.

Fig. 5 shows the infrared spectra of A-series samples. For comparison, the IR spectra of samples **HT-1** and **HT-2** have also been included.

The IR spectrum of **HT-2** catalyst is characterized by the presence of an intense band at 924 cm^{-1}, two broad bands at 750 and 560 cm^{-1}, and a low intense band at 455 cm^{-1} (Fig. 5, spectrum e). This spectrum is very similar to that previously reported for a MoVTeO sample presenting pure M2 phase [35]. Thus, the presence of these bands seems to be characteristic of M2-like crystals.

Table 2
Surface composition and binding energies of Mo $3d_{5/2}$, V $2p_{3/2}$ and Sb $3d_{3/2}$ in MoVSbO catalysts.

Catalyst	Binding energies (eV) and FWHM[a]			Surface composition		
	Mo $3d_{5/2}$	V $2p_{3/2}$	Sb $3d_{3/2}$	Mo	V	Sb
A-1	232.5 (2.10)	516.6 (2.01)	540.6 (1.80)	1.00	0.20	1.00
A-2	232.5 (2.11)	516.6 (1.63)	540.5 (1.77)	1.00	0.15	0.68
A-3	232.6 (2.12)	516.8 (1.74)	540.6 (1.69)	1.00	0.12	0.31
HT-1	232.9 (2.11)	516.7 (1.80)	539.8 (1.68)	1.00	0.18	0.10
HT-2	232.9 (2.05)	516.6 (1.75)	540.1 (1.90)	1.00	0.18	0.49
A-3W	232.9 (3.17)	–	540.8 (2.4) 539.6 (2.2)	0.02	–	1.00

[a] Binding energies at peak maximum and peak half widths (FWHM) of the V $2p_{3/2}$, Mo $3d_{5/2}$ and Sb $3d_{3/2}$ core level lines in the XPS spectra of the catalysts. In parenthesis peak half widths (FWHM) of each element.

The IR spectra of **A-1**, **A-2** and **A-3** samples show the most characteristic bands at 918, 870, 805, 715, 650 and 602 cm^{-1} (Fig. 5, spectra a to c, respectively). Since IR spectrum of sample **HT-1** (with M1 and M2 phases) presents the same bands of **A**-series samples in addition to those related to M2 phase, it can be concluded that bands at 918, 870, 805, 715, 650 and 602 cm^{-1} are related to the presence of M1 phase. The intense bands at 924 or 918 cm^{-1} (from M2 or M1 crystals, respectively) are likely related to the M–Ot bond (M = Mo, V) (Ot, terminal oxygen) [39,40], whilst bands at 870, 805, 715 and 650 cm^{-1}, observed in M1-containing catalysts, are very likely related to antisymmetric vibrations of Mo–O–X (X = Mo, Sb) bridging bonds [39,40]. The band at 750 cm^{-1} could be assigned to asymmetric stretching Mo–Ob bonds (Ob, oxygen is not coordinating Sb inside hexagonal channel), while the band at 455 cm^{-1} corresponds to asymmetric stretching M–Oa–M (M = Mo, V) (Oa, oxygen is coordinating Sb inside hexagonal channel) [40], in M2-like phases.

On the other hand, the absorption bands in the region of 650–550 cm^{-1} are characteristics of antimony oxides [41]. So, the band at 650 cm^{-1} can be also assigned for stretching bending of O–Sb–O while the band at 560 cm^{-1} can be assigned to asymmetric stretching Sb–O–M_2 (M = Mo, V) [42].

Binding energies at peak maximum (BEs) and peak half widths (FWHM) of the V $2p_{3/2}$, Mo $3d_{5/2}$ and Sb $3d_{3/2}$ core level lines in the XPS spectra of the catalysts, as well as the surface metal atomic ratio determined from XPS, are shown in Table 2. Sample **HT-2** presents a Sb/Mo molar ratio higher than sample **HT-1**, which is in agreement to both, the EDX analysis and the stoichiometries of the crystalline phases, i.e. $(SbO)_2M_{20}O_{56}$ and/or $(Sb_2O)M_6O_{19}$, present in these samples.

A Sb-enrichment on the surface of catalysts can be concluded from the XPS results obtained for samples of **A**-series, although Sb/Mo ratio decreases when increasing the number of washing cycles. This is in agreement with the other characterization results shown here and confirms the presence of ($Mo_{0.01-0.02}SbO_{1.9-3.3}{\cdot}xH_2O$) nanoparticles on the surface of M1 phase in these catalysts as a consequence of the elimination of M2 phase during the treatment with an aqueous solution of hydrogen peroxide. Thus, it appears that the presence of Sb species strongly depends on the number of washing cycles. However, also in the sample in which it is not possible to observe the presence of the Sb-rich nanoparticles (as occurs in sample **A-3**), an important contamination of Sb on the surface of M1 phase can be observed (Table 2).

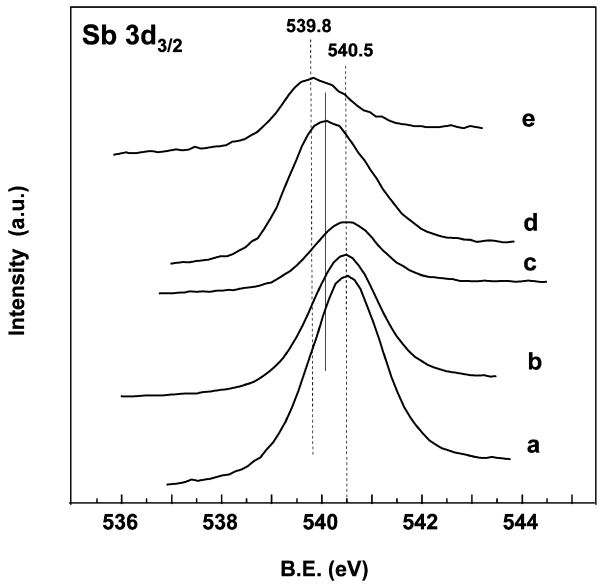

Fig. 6. XPS spectra of Sb $3d_{3/2}$ in MoVSbO based catalysts: (a) **A-1**; (b) **A-2**; (c) **A-3**; (d) **HT-1**; (e) **HT-2**.

On the other hand, a modification of the oxidation state of antimony is also observed in catalysts prepared by the post-synthesis treatment. Thus, the samples prepared hydrothermally and heated in N_2 flow (i.e. **HT-1** and **HT-2**) present mainly Sb^{3+} species on the catalyst surface with binding energies for Sb $3d_{3/2}$ at *ca.* 540.0 eV, while samples prepared by post-synthesis treatment (**A**-series) present mainly Sb^{5+} species on the catalyst surface with binding energies for Sb $3d_{3/2}$ at *ca.* 540.6 eV (see Fig. 6) [27,47].

In addition, in Table 2 are included the XPS results obtained for **A-3W** sample (representative of A-W-series solids). These results confirm the homogeneous stoichiometry of the Sb-rich nanospheres, since it agrees with the composition obtained by EDX. Moreover, it must be commented that a deconvolution of Sb $3d_{3/2}$ signal shows a mixed oxidation state of Sb (77% of Sb^{3+} and 23% of Sb^{5+} with binding energies at *ca.* 539.6 and 540.8 eV, respectively) in the **A-3W** solid.

In the case of Mo and V, no apparent modifications of their corresponding oxidation states have been observed between samples obtained hydrothermally or those achieved after the post-synthesis treatment with an aqueous solution of hydrogen peroxide. The V $2p_{3/2}$ core level signal appears at 516.6 eV in almost all the studied samples. This value is ~0.4 eV lower than that generally reported for pure V_2O_5. However, some authors report a binding energy of 516.6 eV for vanadium (V) [43,44], while binding energies at 516.3, 515.7, 515.6 and 515.4 eV have been reported for the V $2p_{3/2}$ signal in V_6O_{13}, VO_2, V_2O_4 and V_2O_3, respectively [43]. In the case of a phase mixture $V_6Mo_4O_{25}$–MoO_3–As_2O_3, a value of 516.6 eV for the V $2p_{3/2}$ signal was reported [45]. We must indicate that the oxidation state of vanadium atoms in V_6O_{13} is formally 4.33 and the shift to V(V) is only 0.3 eV. V_6O_{13} is slowly formed by heating in vacuum from V_2O_5 [46], but the reduction of V(V) does not occur in He atmosphere up to temperatures of 600 °C [44]. It must be noted that a salt of V^{4+} was used as a precursor for the synthesis of these catalysts and the presence of V(IV) as minority cannot be completely ruled out.

On the other hand, the chemical shift between Mo(VI) and Mo(V) is 1.1 eV. This implies that Mo unequivocally is present in all our samples mainly as Mo(VI) (see Table 2) [44]. However, the observed broadening of the Mo $3d_{5/2}$ signal could suggest some minority presence of Mo cations with an oxidation state lower than +6.

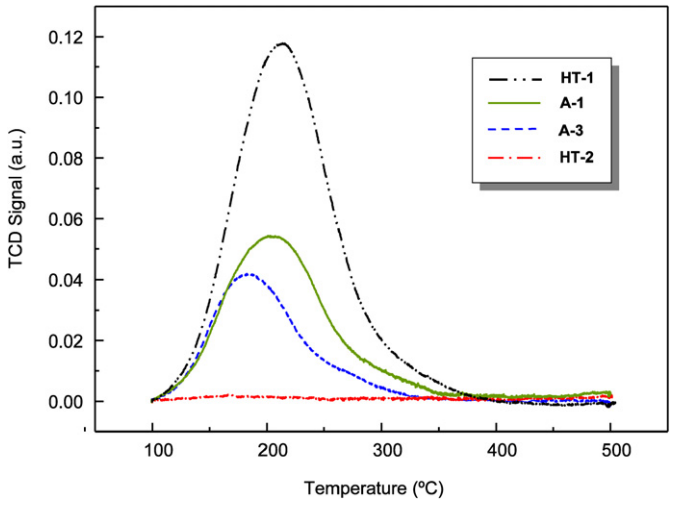

Fig. 7. TPD-NH_3 profiles of catalysts **A-1**, **A-3**, **HT-1** and **HT-2**.

The NH_3-TPD results are summarized in Table 1, while the NH_3-TPD profiles are shown in Fig. 7. According to these results sample **HT-1** presents the highest number of acid sites (320 $\mu mol_{NH_3}\, g^{-1}$, which corresponds to 24 $\mu mol_{NH_3}\, m^{-2}$); while a drastic reduction of the number of acid sites can be inferred in the case of samples obtained by post-synthesis treatment, i.e. **A**-series. This important decrease in the number of acid sites of washed samples, especially when considering the surface area of catalysts (*ca.* 8 $\mu mol_{NH_3}\, m^{-2}$) (Table 1), suggests that the post-synthesis treatment favors a drastic elimination of acid sites on the surface of the catalyst. However, it is difficult at the moment indicating if this drastic reduction of the number of acid sites is related to the elimination of M2 phase or is a consequence of modifications on the surface of M1-phase during the post-synthesis treatment.

It must be informed that the temperature of maximum desorption is remarkably lower in the **A**-series than in the **HT-1** catalyst (Table 1 and Fig. 7). This means that the strength of acid sites decreases after the post-synthesis treatment with aqueous solution of H_2O_2. Moreover, differences among **A**-series catalysts are also observed, decreasing the acid strength as the number of washing cycles increases. In this way, **A-3** catalyst presents both the lowest amount and the lowest strength of acid sites.

On the other hand, the sample **HT-2** presents the lowest number of acid sites (3.7 $\mu mol_{NH_3}\, g^{-1}$), probably as a consequence of both the low surface area and the low specific acidity (*ca.* 1 $\mu mol_{NH_3}\, m^{-2}$). It must be indicated that the average particle size of M2 crystals is much higher in **HT-2** sample (M2 phase alone) than in **HT-1** (a mixture of M1 and M2 crystals).

3.2. Catalytic results

Table 3 shows the catalytic results obtained during the propane oxidation over Mo–V–Sb–O catalysts. Acrylic acid, acetic acid, propylene and carbon oxides were the main reaction products detected in the oxidation of propane. Traces of acrolein, acetaldehyde and acetone were also identified.

HT-1 catalyst (containing both M1 and M2 phases) presents high activity in propane oxidation but low selectivity to acrylic acid, while **HT-2** catalyst (presenting pure M2 phase) is inactive in the propane oxidation.

Strong differences have been observed in the case of samples obtained by post-synthesis treatment (**A**-series catalysts) depending on the number of washing cycles. Fig. 8 shows the variation of the propane conversion with the reaction temperature over these catalysts. For comparison the results obtained over **HT-1** catalysts

Table 3
Oxidation of propane at 380 °C over MoVSb-based catalysts.

Catalyst	Conversion[a] (%)	Selectivity[b] (%)						Areal reaction rate[c]	STY_{AA}[d]
		Acrylic acid	Acetic acid	Propylene	Acetone	CO	CO_2		
A-1	8.5	18.0	6.7	23.2	1.2	27.1	23.7	9.4	5.5
A-2	17.1	38.7	6.0	13.9	0.8	18.9	21.8	20.7	23.8
A-3	23.8	56.1	4.9	11.1	1.4	13.1	13.2	33.1	48.1
HT-1	25.4	13.4	13.8	8.8	1.1	29.4	33.5	41.9	12.3
HT-2	< 0.2								

[a] Propane conversion at reaction temperature of 380 °C, and a contact time, W/F, of 200 $g_{cat.}\,h\,(mol_{C_3H_8})^{-1}$.
[b] Selectivity to reaction products (in some experiments acetaldehyde and acrolein were also observed but with selectivity below 0.2%).
[c] Areal reaction rate expressed in 10^4 $g_{C_3H_8}\,h^{-1}\,m^{-2}$ (S_{BET} data in Table 1).
[d] Rate of formation of acrylic acid (AA) per unit mass of catalyst and per unit time, STY_{AA}, in $g_{AA}\,h^{-1}\,kg_{cat.}^{-1}$.

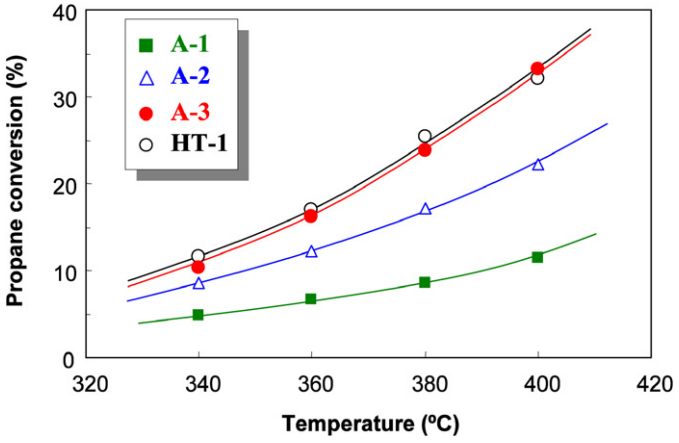

Fig. 8. Variation of propane conversion with the reaction temperature obtained during the oxidation of propane over MoVSbO based catalysts: **A-1** (■); **A-2** (△); **A-3** (●); **HT-1** (○). Reaction conditions: $C_3H_8/O_2/He/H_2O$ molar ratio of 4/8/58/30, $W/F = 200\ g_{cat.}\,h\,mol_{C_3H_8}^{-1}$.

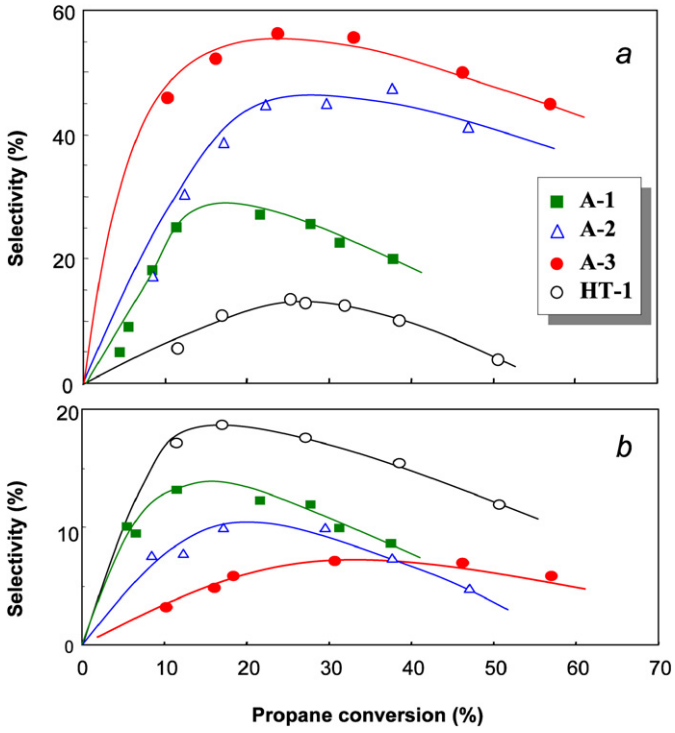

Fig. 9. Variation of the selectivity to acrylic acid (a) and acetic acid (b) with the propane conversion obtained during the oxidation of propane over MoVSbO based catalysts. Reaction conditions in the text; symbols: **A-1** (■); **A-2** (△); **A-3** (●); **HT-1** (○).

are also included. The catalytic activity for propane oxidation increases when increasing the number of washing cycles, with catalysts **A-3** and **HT-1** presenting similar catalytic activity for propane oxidation.

Fig. 9 shows the variation of the selectivity to acrylic acid (Fig. 9a) and acetic acid (Fig. 9b) with the propane conversion obtained at 380 °C on pure and mixed phases. For post-treated samples, the selectivity to acrylic acid increases when increasing the number of washing cycles, while the selectivity to acetic acid presents an opposite trend to that observed for the selectivity to acrylic acid. We must indicate that **HT-1** catalyst has been the most selective catalyst to acetic acid and the less selective to acrylic acid.

Accordingly, pure orthorhombic M1-containing catalysts are very active and selective in the oxidation of propane to acrylic acid, although both the activity for propane oxidation and the selectivity to acrylic acid strongly depend on the number of washing cycles after the post-synthesis treatment with aqueous solution of hydrogen peroxide. In this way, it is interesting to remark that **A-3** catalyst presents selectivity to acrylic acid of *ca.* 57% at a propane conversion of 30% (at reaction temperature of 380 °C and contact time, W/F, of 200 $g_{cat.}\,h\,mol_{C_3H_8}^{-1}$).

Table 3 presents also the reaction rates (obtained at 380 °C) per unit surface area for untreated and post-synthesis treated catalysts. The areal reaction rate for **A**-series catalysts increases as increasing the number of washing cycles, although these ones are lower than that observed for sample **HT-1**. However, if we consider the rate of formation of acrylic acid per unit mass of catalyst and per unit time, STY_{AA} (space time yield), it can be seen that the higher acrylic acid formation is obtained during the propane oxidation over the M1-pure based catalysts, especially over **A-3** sample. Moreover, it must be considered that this catalyst (**A-3**) shows a STY_{AA} similar to those achieved over MoVTeNb catalysts [19].

Table 4 shows comparatively the catalytic results obtained during the oxidation of propylene over MoVSbO catalysts. Acrylic acid, acetic acid, acrolein, acetone and carbon oxides were the main reaction products, although traces of acetaldehyde were also observed.

As observed in propane oxidation, the post-synthesis treated samples, i.e. **A**-series, show also high activity and selectivity to acrylic acid during the oxidation of propylene. In this way, both propylene conversion and the areal reaction rate increase with the number of washing cycles. However, although following the same trend, low differences in the selectivity to acrylic acid have been observed for **A**-series catalysts.

At this point we must inform that a STY_{AA} of 275 $g_{AA}\,h^{-1}\,kg_{cat.}^{-1}$ is achieved during the selective oxidation of propylene over **A-3** sample.

Moreover, it must be indicated that **HT-1** catalyst (containing both M1 and M2 phases) presents high activity in propylene oxidation and a relatively high selectivity to acrylic acid, meanwhile

Table 4
Oxidation of propylene on MoVSb-based catalysts.

Catalyst	W/F[a]	Conversion[b] (%)	Selectivity[c] (%)					Areal reaction rate[d]	STY_{AA}[e]
			Acrylic acid	Acetic acid	Acetone	CO	CO_2		
A-1	150	27.5	68.8	0.3	8.3	18.1	4.3	37.4	90.8
A-2	150	66.4	73.3	3.9	4.5	12.6	5.5	102	234
A-3	150	74.8	76.7	2.1	1.0	13.7	6.5	133	275
HT-1	150	65.8	38.1	15.0	8.7	26.4	11.9	140	120
HT-2	480	36.7	0	27.9	15.9	42.6	12.5	94.4	0

[a] Contact time, W/F, in $g_{cat.}\,h\,(mol_{C_3H_6})^{-1}$.
[b] Propylene conversion at 380 °C.
[c] Selectivity to reaction products (acetaldehyde and acrolein were observed in some experiments although with selectivity lower than 0.5%).
[d] Areal reaction rate at 380 °C expressed in 10^4 $g_{C_3H_6}\,h^{-1}\,m^{-2}$ (S_{BET} data in Table 1).
[e] Rate of formation of acrylic acid (AA) at 380 °C per unit mass of catalyst and per unit time, STY_{AA}, in $g_{AA}\,h^{-1}\,kg_{cat.}^{-1}$.

HT-2 catalyst (containing only the M2 phase) presents a low activity in propylene oxidation and is unselective in the formation of acrylic acid. So it is clear that the elimination of the M2 phases could have a positive effect on the catalytic behavior of these catalysts.

3.3. On the role of M1 and M2 phase in MoVSbO mixed oxide catalysts

It is known that the M2 phase, in both Nb-free and Nb-containing Mo–V–Te–O catalysts, is inactive in propane oxidation but it is active and selective in the partial oxidation of propylene to acrolein or acrylic acid, respectively [35]. This could explain a possible synergism with M1 phase during the propane partial oxidation over MoVTeNbO catalysts [24,25]. Accordingly, the presence of the M2 phases could have a positive influence on the catalytic behavior of these catalysts.

In the case of Nb-free Mo–V–Sb–O catalysts the role of M2 phase is not clear and seems to be quite different, since according to the results presented here, this phase shows a poor selectivity to partial oxidation products during the propene oxidation (Table 4). Thus, one first approach to explain the poor results of MoVSbO catalysts containing both M1 and M2 phases could be related to a negative influence of M2 phase (in an opposite trend to that proposed in the case of MoVTeO) catalysts. However we can neither discard that these poor results achieved over sample **HT-1** could be related to the worse catalytic performance of M1 phase by itself. In fact, the better selectivity to acrylic acid of pure M1 phase based catalysts seems to be associated to the changes on the surface of this phase as a consequence of the post-synthesis treatment with aqueous H_2O_2 solution. Thus, it has been evidenced that the elimination and the modification of acid sites observed by NH_3-TPD on the catalyst surface of **A**-series, probably due to surface Sb enrichment (as shown by XPS results), favors a higher formation of acrylic acid. In the same way, it is known that the incorporation of K or Nb in MoVSbO mixed oxides favors both, an elimination of the surface acid sites and an improvement of the catalytic behavior [15,23,25,30,31].

According to the characterization results presented here, three important modifications on the surface of the catalysts of the **A**-series are observed if compared to sample **HT-1**: (i) a drastic decrease in the number of acid sites, (ii) a Sb-enrichment of the catalyst surface, and (iii) a modification of the oxidation state of antimony on the catalyst surface. Thus, the changes observed in samples obtained by post-synthesis treatment can be related to the elimination of acid sites by leached antimony species (obtained from the M2 phase decomposition during the post-synthesis treatment) on the catalysts surface. However, the optimal amount of Sb on the catalyst surface should have a limit. This limit must be related to the number of acid sites on the catalyst surface, while an excess of antimony species could also block the active sites for alkane activation favoring a decrease in the catalytic activity. If this is so, it is not surprising that increasing the number of washing cycles we can decrease the amount of both the ($Mo_{0.01-0.02}SbO_{1.9-3.3}\cdot xH_2O$) nanospheres and leached antimony species deposited over catalyst surface, increasing thus the alkane conversion.

As it has been already indicated, the oxidation state of antimony species on the surface of solids changes during the post-synthesis treatment with aqueous solution of hydrogen peroxide. Thus Sb^{3+} is only observed in samples **HT-1** and **HT-2** (Table 2) in agreement to previous results [30], while Sb^{5+} is mainly observed in catalysts of **A**-series. Although the best catalytic performance of post-synthesis treated samples (containing pure M1 phase) could be also related to the higher oxidation state of antimony in the catalysts; a similar improvement is obtained on potassium doped MoVSbO catalysts, and no important variation of the oxidation state of antimony species on the catalysts surface is observed [30]. In this way, Millet et al. have proposed that the Sb atoms in M1 phase have a high versatility and its oxidation state can change independently of the catalytic behavior [48].

Finally, we must comment that the influence of the post-synthesis treatment on the catalytic behavior of MoVSbO is different to that recently observed over MoVTeNbO catalysts [25]. In our case, the post-synthesis treatment with aqueous H_2O_2 solution improves the selectivity to acrylic acid, with a relatively low loss of the catalytic activity in the best case, **A-3** catalyst. In a different way, the post-synthesis treatment with an aqueous H_2O_2 solution of MoVTeNbO catalysts is reported to favor an increase in the catalytic activity without changes in the selectivity to acrylic acid [25].

4. Conclusions

At the present paper highly active and selective Nb-free MoVSb catalysts have been prepared by a post-synthesis procedure: heat-treated MoVSb solids, previously obtained hydrothermally, are treated with aqueous H_2O_2 solutions. Using these catalysts, yields to acrylic acid of *ca.* 30% have been attained, which represents an important improvement compared to those previously reported on MoVSb mixed oxides [27–31,34]. However, the catalytic behavior of these catalysts strongly depends on the washing procedure.

The characterization results of catalysts prepared by a post-synthesis treatment suggest that the M2 phase is completely removed, and M1 phase is mainly present. However, in samples poorly washed, Sb-rich nanoparticles ($Mo_{0.01-0.02}SbO_{1.9-3.3}\cdot xH_2O$) on the surface of M1 crystals are also observed.

The results presented here demonstrate that the role of the M2-type crystalline phase in MoVSbO catalysts is completely different to that previously proposed for MoVTeNbO catalysts. In the case of Sb-based catalysts, the M2 phase presents a poor selectivity to partial oxidation products during the oxidation of propene. However,

this aspect cannot explain completely the poor catalytic results obtained during the selective oxidation of propane to acrylic acid over Nb-free Mo–V–Sb–O catalysts.

Since a drastic elimination of the number of acid sites took place on the catalyst surface of Mo–V–Sb–O catalysts modified by a post-synthesis treatment, it can be concluded that killing the acid sites present on the catalysts could be an attractive route to the preparation of selective catalysts. This is in agreement to previous results obtained over K-doped MoVSbO catalysts, although in our case the catalytic improvement is obtained through an apparently selective incorporation of Sb species during the post-synthesis treatment.

Moreover, we consider the results presented in this work are of significant importance since the chemical composition and the operation conditions of the catalytic reaction could be further optimized.

Acknowledgments

The authors thank the Spanish CICYT for financial support (Projects NAN2004-09267-C03-02 and CTQ2006-09358/BQU) and the technical support of the Microscopy Department of Universidad Politécnica de Valencia (Spain).

References

[1] T. Ushikubo, Catal. Today 57 (2000) 331.
[2] M.M. Lin, Appl. Catal. A Gen. 207 (2001) 1.
[3] R.K. Grasselli, J.D. Burrington, D.J. Buttrey, P. DeSanto, C.G. Lugmair, A.F. Volpe, T. Weingand, Top. Catal. 23 (2003) 5.
[4] D. Vitry, J.L. Dubois, W. Ueda, J. Mol. Catal. A 20 (2004) 67.
[5] J.M. López Nieto, Top. Catal. 41 (2006) 3.
[6] T. Ushikubo, I. Sawaki, K. Oshima, K. Inumaru, S. Kovayakawa, K. Kiyono, EP 0,603,836 (1993), US Patent 5,442,328 (1993).
[7] T. Ushikubo, H. Nakamura, Y. Koyasu, S. Wajiki, US Patent 5,380,933 (1995), EP 0,608,838 B1 (1997).
[8] T. Ushikubo, K. Oshima, A. Kayou, M. Hatano, Stud. Surf. Sci. Catal. 112 (1997) 473.
[9] J.M. López Nieto, P. Botella, M.I. Vázquez, A. Dejoz, Chem. Commun. (2002) 1906;
J.M. López Nieto, P. Botella, M.I. Vázquez, A. Dejoz, WO patent 03/064035 (2003).
[10] P. Botella, E. García-González, A. Dejoz, J.M. López Nieto, M.I. Vázquez, J. González-Calbet, J. Catal. 225 (2004) 428.
[11] B. Solsona, M.I. Vázquez, F. Ivars, A. Dejoz, P. Concepción, J.M. López Nieto, J. Catal. 252 (2007) 271.
[12] B. Solsona, F. Ivars, P. Concepción, J.M. López Nieto, J. Catal. 250 (2007) 129.
[13] J.M. M Millet, H. Roussel, A. Pigamo, J.L. Dubois, J.C. Jumas, Appl. Catal. A Gen. 232 (2002) 77.
[14] P. DeSanto, D.J. Buttrey, R.K. Grasselli, C.G. Lugmair, A.F. Volpe, B.H. Toby, T. Vogt, Z. Kristallogr. 219 (2004) 152.
[15] W. Ueda, D. Vitry, T. Katou, Catal. Today 99 (2005) 43.
[16] P. Botella, E. García-González, J.M. López Nieto, J.M. González-Calbet, Solid State Sci. 7 (2005) 507.
[17] (a) H. Tsuji, K. Oshima, Y. Koyasu, Chem. Mater. 15 (2003) 2112;
(b) H. Tsuji, Y. Koyasu, J. Am. Chem. Soc. 124 (2002) 5608.
[18] P. Korovchenko, N.R. Shiju, A.K. Dozier, U.M. Graham, M.O. Guerrero-Pérez, V.V. Guliants, Top. Catal. 50 (2008) 43.
[19] P. Botella, J.M. López Nieto, B. Solsona, A. Mifsud, F. Márquez, J. Catal. 209 (2002) 445.
[20] B. Solsona, J.M. López Nieto, J.M. Oliver, J. Gumbau, Catal. Today 91–92 (2004) 247.
[21] (a) D. Vitry, Y. Morikawa, J.L. Dubois, W. Ueda, Top. Catal. 23 (2003) 47;
(b) D. Vitry, Y. Morikawa, J.L. Dubois, W. Ueda, Appl. Catal. A 251 (2003) 411.
[22] A. Celaya Sanfiz, T.W. Hansen, A. Sakthivel, A. Trunschkle, R. Schlöhl, A. Knoester, H. Brongersma, M.H. Looi, S.B.A. Hamid, J. Catal. 258 (2008) 35.
[23] W. Ueda, K. Oshihara, D. Vitry, T. Hisano, Y. Kayashima, Catal. Surv. Jpn. 6 (2002) 33.
[24] J. Holmberg, R.K. Grasselli, A. Andersson, Appl. Catal. A 270 (2004) 121.
[25] (a) M. Baca, M. Aouine, J.L. Dubois, J.M.M. Millet, J. Catal. 233 (2005) 234;
(b) B. Deniau, G. Bergeret, B. Jouguet, J.L. Dubois, J.M.M. Millet, Top. Catal. 50 (2008) 33.
[26] J.M.M. Millet, M. Baca, A. Pigamo, D. Vitry, W. Ueda, J.L. Dubois, Appl. Catal. A 244 (2003) 359.
[27] J.C. Vedrine, E.M. Novakova, E.G. Derouane, Catal. Today 81 (2003) 27.
[28] J.N. Al-Saeedi, V.V. Guliants, O. Guerrero-Pérez, M.A. Bañares, J. Catal. 215 (2003) 108.
[29] V.V. Guliants, R. Bhandari, H.H. Brongersma, A. Knoester, A.M. Gaffney, S. Han, J. Phys. Chem. B 109 (2005) 10234.
[30] (a) T. Blasco, P. Botella, P. Concepción, J.M. López Nieto, A. Martínez-Arias, C. Prieto, J. Catal. 228 (2004) 362;
(b) P. Botella, P. Concepción, J.M. López Nieto, B. Solsona, Catal. Lett. 89 (2003) 249.
[31] W. Ueda, Y. Endo, N. Watanabe, Top. Catal. 38 (2006) 261.
[32] P. Concepción, P. Botella, J.M. López Nieto, Appl. Catal. A Gen. 278 (2004) 45.
[33] P. Botella, A. Dejoz, J.M. López Nieto, P. Concepción, M.I. Vázquez, Appl. Catal. A Gen. 298 (2006) 16.
[34] M. Baca, A. Pigamo, J.L. Dubois, J.M.M. Millet, Catal. Commun. 6 (2005) 215.
[35] P. Botella, J.M. López Nieto, B. Solsona, Catal. Lett. 78 (2002) 383.
[36] H. Hibst, F. Rosowski, G. Cox, Catal. Today 117 (2006) 234.
[37] M. Baca, J.M.M. Millet, Appl. Catal. A Gen. 279 (2005) 67.
[38] J.N. Al-Saeedi, V.K. Vasudevan, V.V. Guliants, Catal. Commun. 4 (2003) 537.
[39] J.C.J. Bart, F. Cariati, A. Sgamelloti, Inorg. Chim. Acta 48 (1981) 97.
[40] M.H. Alizadeh, A.R. Salimi, Spectrochim. Acta A 65 (2006) 1104.
[41] R. Nilsson, T. Lindblaud, A. Andersson, J. Catal. 148 (1994) 501.
[42] R. Grabowski, A. Gumuka, J. Sloczynski, J. Phys. Chem. Solids 41 (1980) 1027.
[43] S.L.T. Anderson, J. Chem. Soc. Faraday Trans. 75 (1979) 1356.
[44] L.Z. Zhao, S.H. Lui, D.H. Wang, C.H. Pan, J. Electron Spectrosc. Relat. Phenom. 52 (1990) 571.
[45] G. Hopfengärtner, D. Borgmann, I. Rademacher, G. Wedler, E. Hums, G.W. Spitznagel, J. Electron Spectrosc. Relat. Phenom. 63 (1993) 91.
[46] R.J.D. Tilley, B.G. Hyde, J. Phys. Chem. Solids 30 (1970) 1613.
[47] R. Reiche, D. Dobler, J.P. Holgado, A. Barranco, A.I. Martín-Concepción, F. Yubero, J.P. Espinós, A.R. González-Felipe, Surf. Sci. 537 (2003) 228.
[48] O.V. Safonova, B. Deniau, J.M.M. Millet, J. Phys. Chem. B 110 (2006) 23962.